Charge transport across dynamic covalent chemical bridges

Zelin Miao,[a] Timothy Quainoo,[b] Thomas M. Czyszczon-Burton,[a] Nils Rotthowe,[a] Joseph M. Parr,[a] Zhen-Fei Liu,[b]* and Michael S. Inkpen[a]*

[a] *Department of Chemistry, University of Southern California, Los Angeles, California 90089, United States*

[b] *Department of Chemistry, Wayne State University, Detroit, Michigan 48202, United States*

E-mail: zfliu@wayne.edu, inkpen@usc.edu

ABSTRACT

Dynamic covalent chemistry (DCC) plays a critical role in the preparation of extended polymeric materials such as covalent-organic frameworks (COFs). Using DCC, the formation of targeted equilibrium, rather than kinetic, products are driven by the error-correcting capabilities of the reversible bond forming reactions involved. As work to develop *conductive* COFs (and metal-organic frameworks, MOFs) intensifies, it is of increasing interest to characterize the electronic transparency of bridge motifs formed from different DCC reactions. Here we apply the scanning tunneling microscope-based break junction (STM-BJ) method to measure the conductance of atomically-precise molecular junctions comprising imine, imidazole, diazaborole, and boronic ester bridge groups. Their comparison is facilitated through utilization of a glovebox-based STM-BJ setup operating under an inert atmosphere that avoids the apparent hydrolysis of boronic ester-containing compounds when these are studied in air. We find that junction transport generally increases as the difference in electronegativity ($\Delta\chi$) between bridge group atoms decreases, and that conductance decays most rapidly with distance for compounds comprising boronic esters. Our experimental results are supported by first-principles calculations that reveal a different nodal structure in the transmission eigenchannel in boronic ester-containing systems compared to the other molecules. Taken together, our work reaffirms expectations that highly polarized bridge motifs represent poor choices for the preparation of extended materials with high through-bond electronic conductivity. We propose that such molecular-scale transport studies of "framework fragments" can provide new insights into the intrinsic properties of bulk COF and MOF systems that may be exploited in the design of improved materials.

INTRODUCTION

Covalent-organic frameworks (COFs) are highly modular classes of permanently porous, crystalline two and three dimensional (2D and 3D) organic polymers, assembled using dynamic covalent bond-forming chemistries (DCC). The use of such reversible reaction processes for assembly is key to solving the "crystallization problem," avoiding the formation of disordered, amorphous 2D and 3D kinetically trapped products that lie far from their thermodynamic minima.[1–3] Accordingly, prior to any potential post-synthetic modification(s), the molecular groups or coordination bonds formed during assembly are present as fundamental structural elements of all crystalline COFs or metal-organic frameworks (MOFs, related materials comprising metals). While such connective elements can be used exclusively for linking together other components at specific angles to form a desired framework topology or pore size(s), they have the potential to play a larger role in framework function where their identity impacts electronic structure. Their properties are therefore important when designing COFs and MOFs with specific electrical properties for applications in areas such as electrocatalysis,[4,5] electrically-transduced chemical sensing,[6,7] or energy storage.[8–12] Electronic transport in these bulk materials is ideally characterized through four-point probe/van der Pauw measurements of pressed pellet[13] or single-crystal[14–16] samples, with conductivity trends assessed in terms of through-bond/extended conjugation, through-space, or redox-hopping mechanisms.[17,18] However, the systematic comparison of different materials, as well as the unambiguous determination of structure-property relationships, is challenging due to variations in framework topology, composition, and the number and type of defects.[17] Despite such challenges, seminal early work showed that hole mobilities for imine-bridged porphyrin-based COFs were higher than for a structurally similar COF with boronic ester linkages (8.1 and 3.0 $cm^2\ V^{-1}\ s^{-1}$, respectively).[19]

Here we pursue a bottom-up strategy to probe the intrinsic electronic properties of molecule-based framework materials by measuring the conductance of "framework fragments", model molecular species with framework-inspired chemical structures. Such measurements directly address through-bond transport in atomically precise single-molecule junctions. This approach can be considered a particular form of *dimensional reduction*, where, for example, 3D bulk materials are broken down into 2D, 1D, or 0D forms to provide a deeper understanding of their properties.[20,21] Examples of dimensional reduction studies relevant to frameworks include the collection of infrared spectra for discrete boronic acid, boroxine anhydride, and boronate ester species to facilitate spectral analyses of bulk materials,[22]

scanning probe investigations of surface-supported 2D COFs,[23,24] and the use of "0D" triphenylene-based Cu or Co compounds to probe spin interactions, inter-site electronic couplings, or out-of-plane interactions in 2D MOFs.[25–27] While charge-hopping processes,[28,29] through-space interactions,[19,30–33] and topological effects on band structures[34–37] complicate the transfer of any 1D molecular tunneling conductance trends to extended materials of higher dimensionality, connections between molecular orbitals and bulk band structures are well established.[38] Interestingly, recent transport studies of thioether-terminated oligosiloxanes[39] have shown that these molecular analogues of the bulk insulator silicon dioxide are among the least conductive molecular wires known. Conductance measurements on molecular fragments relevant to conducting polymers and polyaromatic hydrocarbons have also been targeted to provide insights into the nature of their corresponding macroscopic systems.[40,41] From a practical standpoint, some framework fragments might be considered too unstable to study outside of the bulk. However, it may still be possible to characterize transient species. This was demonstrated in an investigation of metal-bridged, 1,4-bis(isocyano)benzene-based oligomeric wires formed *in situ*, which were proposed as model systems to interrogate the conducting properties of coordination polymers/MOFs.[42]

In this work we synthesize and study a series of isolable model compounds comprising thioether electrode linkers connected by one or two imine[43] (**2CN** or **2CN-L**), imidazole[44] (**CN** or **CN-L**), diazaborole[45] (**BN** or **BN-L**), or boronic/boronate ester[46] (**BO** or **BO-L**) bridge groups (**Figures 1c**, **2a**, and **4a;** "**L**" = long and "**2**" = number of bridge atoms). Each bridge structure has previously been used for the synthesis of porous organic extended frameworks (for an example, see **Figure 1a**). We evaluate charge transport across each bridge group by measuring the single-molecule conductance of these compounds in nanoscale junctions formed using the scanning tunneling microscope-based break-junction (STM-BJ) method (**Figure 1b**, see Methods and the SI for details). Notably, we find that measurements of boronic ester-containing molecules must be performed under an inert atmosphere to avoid their apparent decomposition through hydrolysis. We observe a clear trend between the decreasing conductance (G) of the intact series of model compounds and the increasing difference in electronegativity ($\Delta\chi$) of DCC bridge atoms ($G_{2C\text{-}N} \sim G_{C\text{-}N} > G_{B\text{-}N} > G_{B\text{-}O}$, where $\Delta\chi_{CN} = 0.49 < \Delta\chi_{BN} = 1.00 < \Delta\chi_{BO} = 1.40$ using the Pauling scale), and find that the decay in tunneling conductance with length extension is most rapid in molecules containing boronic ester groups. First-principles calculations using a combination of density functional theory (DFT) and non-equilibrium Green's function (NEGF)[47] corroborate the experimentally observed trends and reveal a different nodal structure in the transmission eigenchannel of **BO**, which serves as a

charge trap that decreases junction conductance. Though this study focuses only on a sub-set of known DCC bridge groups, we stress that our approach can be applied to probe the electronic properties of different families of molecule-based framework fragments – ultimately providing new perspectives on the intrinsic electrical transport properties of their corresponding extended materials.

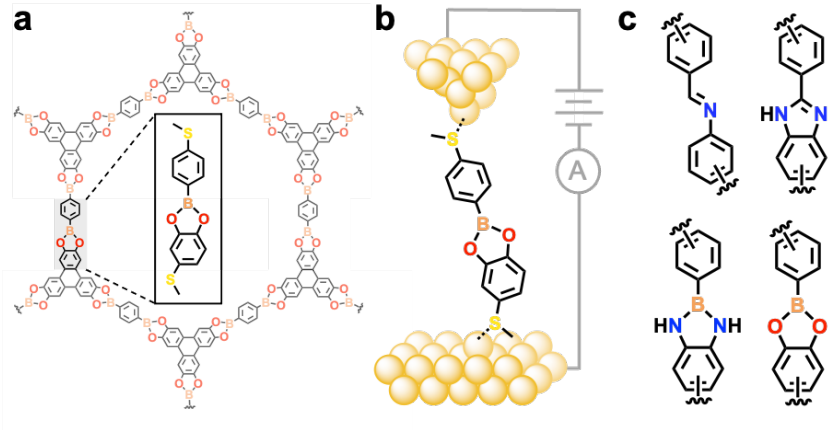

Figure 1. (a) The structure of COF-5, a seminal example of a permanently porous crystalline organic polymer prepared using dynamic covalent chemistry (DCC). In this case, reversible condensation reactions between boronic acids and 1,2-diols lead to the formation of an extended molecular framework comprising alternating phenylene and triphenylene groups linked by boronic ester bridges. *Inset:* the molecular structure of **BO**, a model compound comprising aryl thioether electrode linkers bridged by a single boronic ester group. **(b)** A schematic representation of a nanoscale molecular junction comprising **BO**. Such junctions are formed using the scanning tunneling microscope-based break junction (STM-BJ) method, facilitating single-molecule conductance measurements of different model compounds connected between gold electrodes. **(c)** Molecular structures of imine, imidazole, diazaborole, and boronic ester DCC bridge groups investigated in this study.

RESULTS AND DISCUSSION

The model compounds studied here comprise terminal aryl thioether groups linked by 1 or 2 dynamic covalent chemical (DCC) bridges. Thioether groups were incorporated as they are established electrode linkers for STM-BJ experiments, forming well-defined physical and electrical contacts through selective binding of the sulfur lone pair to undercoordinated gold atoms.[48,49] Importantly, they are also unreactive under the different condensation conditions and chemical transformations used in the preparation of the targeted DCC-bridged compounds. The bridges are formed through their respective condensation reactions, combining: aldehyde and amine groups to form imines, 1,2-diamine and aldehydes to form imidazoles; 1,2-diamine

and boronic acids to form diazaboroles; and 1,2-diols and boronic acids to form boronic esters. Each condensation reaction produces water which is in some cases eliminated through azeotropic distillation with toluene (Dean-Stark method) or reaction with a desiccant such as 3Å molecular sieves, driving chemical equilibria towards formation of the desired products. The precursor 4-(methylthio)benzene-1,2-diamine (**MeS-2N**) was obtained in two steps from 5-chloro-2-nitroaniline. The thioether group was first installed through nucleophilic substitution at the aryl chloride using sodium thiomethoxide (forming **1**), whereby the nitro group was reduced to amine with $SnCl_2$-ethanol. 4-(Methylthio)benzene-1,2-diol (**MeS-2O**) was synthesized from 3-(methylthio)phenol through reaction with paraformaldehyde to form 2-hydroxy-4-(methylthio)-benzaldehyde (**2**), followed by Dakin oxidation of the aldehyde to the *cis*-diol using sodium percarbonate.[50] Detailed synthetic protocols for all molecules are provided in the Supporting Information (**SI**).

We initially apply the STM-BJ method to perform conductance measurements on molecules containing one bridge group (**Figure 1b** and **2a**). In **Figure 2b**, we present overlaid 1D conductance histograms obtained from 1,2,4-trichlorobenzene (TCB) solutions of **BN** and **BO** that have been prepared and measured in air. In each case, we observe a high conductance feature at ~10^{-2} G_0 (where $G_0 = 2e^2/h = 7.748 \times 10^{-5}$ S), in addition to a broad low conductance feature for **BO** and a relatively sharp feature at ~10^{-3} G_0 for **BN**. Further analysis of the 2D conductance-displacement histograms for these experiments (**SI, Figure S2**) reveals the most probable junction length for the 10^{-2} G_0 feature is ~0.6 nm (assuming a "snap back" distance = 0.5 nm[51–53]). This is significantly shorter than the S-S distance (1.1-1.3 nm) in optimized structures obtained from our first-principles calculations of these junctions, detailed below. We propose two hypotheses for the origin of the common 10^{-2} G_0 feature: (1) that **BN** and **BO** decompose via hydrolysis *in situ* to molecular products that can also form junctions; or (2) that **BN** and **BO** remain intact but can contact electrodes through a group other than the thioether substituents. To test the first hypothesis, we measure the hydrolysis products of **BO** and **BN**: 4-(methylthio)phenylboronic acid (**MeS-BO**), **MeS-2O**, and **MeS-2N** (**SI, Figure S3**). Remarkably, 1D histograms for both **MeS-BO** and **MeS-2N** reveal features at comparable conductance and junction displacements, strongly indicating that **BO** and **BN** form these species through hydrolysis during STM-BJ measurements in air. While amines are well-known contact groups in STM-BJ experiments,[54] and boron-containing junctions have previously been studied,[55–60] the ability of boronic acids to act as electrode linkers has not yet been established.

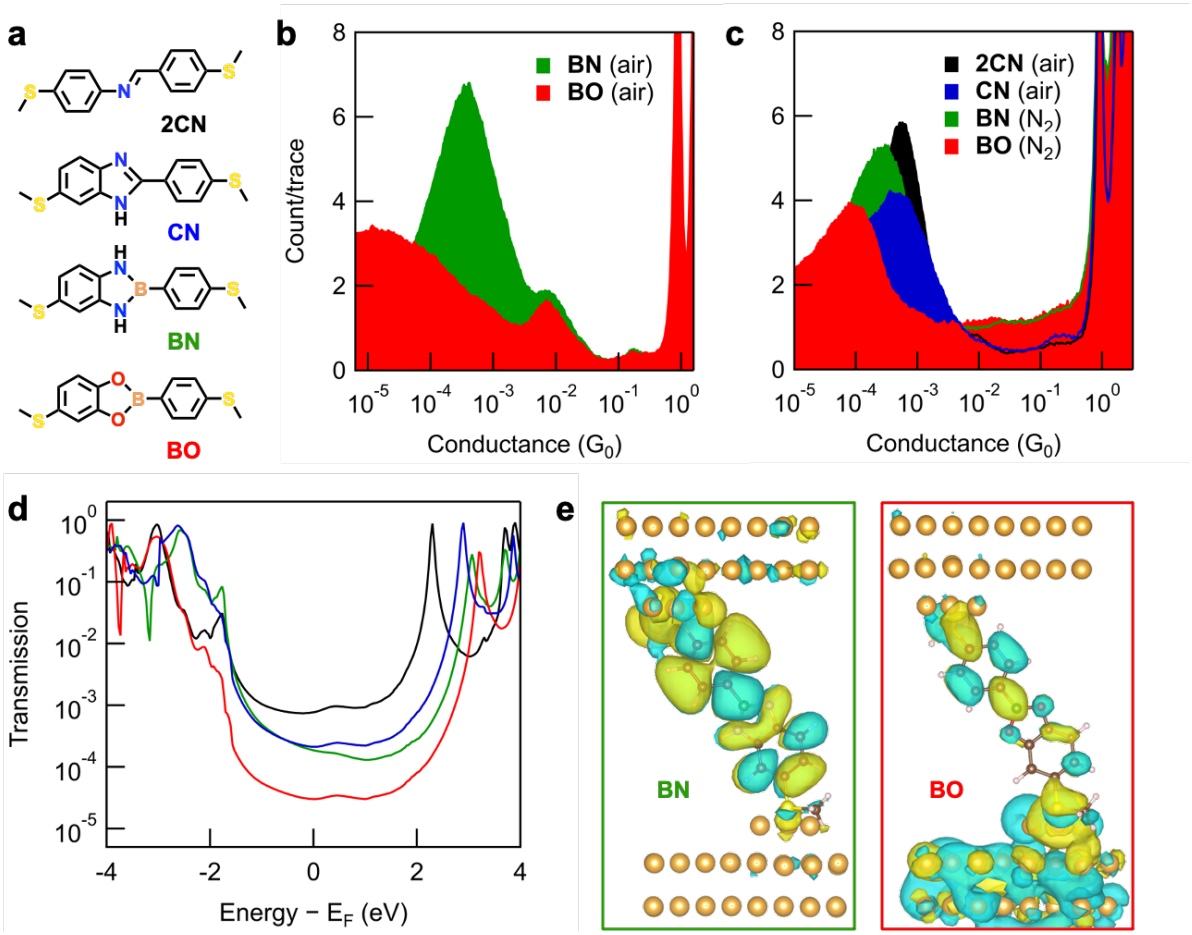

Figure 2. (a) Molecular structures of model compounds containing one DCC bridge group. **CN** has two tautomeric forms but is drawn here with the C=N bond *para* to the terminal thioether group for simplicity. **(b)** Overlaid 1D histograms obtained from measurements of **BO** and **BN** in TCB solutions in air (V_{bias} = 100 mV, 10,000 traces). We assign the common peak at ~10^{-2} G_0 to junctions containing **MeS-BO** and **MeS-2N** which form as these compounds fully or partially hydrolyze (**SI, Figure S3**). **(c)** Overlaid 1D histograms for intact **BN** and **BO** junctions measured under an inert nitrogen atmosphere, and **CN** and **2CN** junctions measured in air (V_{bias} = 100 mV, 10,000 traces). For measurements under inert atmosphere, we attribute the higher counts between ~10^{-2}-10^{0} G_0 to increased interactions between undercoordinated gold atoms and aromatic molecules in the absence of air (see main text and SI for further discussion). **(d)** Transmission functions for the four molecular junctions obtained from NEGF, using the DFT+Σ approach.[61,62] The Fermi energy (E_F) of the junction is set to be zero. LUMO resonance peaks for **CN** and **2CN** (between 2-3 eV above E_F) approach unity, suggesting symmetric conducting orbitals. Those for **BO** and **BN** (around 3 eV above E_F) are much smaller than 1, suggesting asymmetric conducting orbitals. **(e)** Transmission eigenchannels for **BN** and **BO**, evaluated at the LUMO resonance peak. The reduced conductance of **BO**, relative to **BN** is attributed to their different nodal structure and charge localization around the oxygen atom.

To avoid the apparent hydrolysis of **BO** and **BN** during conductance measurements, we subsequently perform STM-BJ experiments in dry, deoxygenated solutions of these molecules

under an inert atmosphere in a dry, nitrogen-filled glovebox (capable of operating at <1 ppm H_2O, <1 ppm O_2). Further details of the operation of this STM-BJ system are provided in the **SI**. In **Figure 2c** we plot overlaid 1D conductance histograms for **BO** and **BN** measured under an inert atmosphere, as well as for **CN** and **2CN** measured in air. Each shows a single conductance peak as well as the conspicuous *absence* of features at 10^{-2} G_0. Their corresponding 2D conductance-displacement histograms also reveal significantly longer most probable junction lengths (**SI, Figure S10**). This clearly indicates that **BO** and **BN** are stable when measured under anhydrous conditions, that **CN** and **2CN** do not hydrolyze during measurement in air, and that the dominant conductance peaks in these histograms correspond to junction geometries where molecules are bound to electrodes via both thioether substituents (further negating hypothesis 2, above). We note that the poorly defined low conductance feature initially observed for **BO** (**Figure 2b**) has been replaced by a new well-defined peak at ~10^{-4} G_0 (**Figure 2c**). We propose that this new peak originates from measurement of the intact **BO** junction and attribute its initial absence (**Figure 2b**) to the decomposition of **BO** when its solutions are prepared and measured in air (in line with hypothesis 1, above). No persistent conductance peak is observed even when **BO** solutions are first prepared in anhydrous, oxygen-free TCB inside the glovebox then measured in air (**SI, Figure S4**). This indicates that a sustained inert atmosphere is critical to the formation and measurement of intact **BO** junctions. In contrast to the **BO** measurements the primary conductance feature at ~10^{-3} G_0 for **BN** is present in histograms constructed from both air and glovebox measurements, suggesting that **BN** only partially hydrolyzes when studied in air. Overlaid histograms for **BN** and **2CN** junctions measured in air and in a nitrogen-filled glovebox show that their conductance is not significantly impacted by the presence or absence of water and/or oxygen (**SI, Figure S5**). Despite recent reports of molecular junctions comprising imidazole-based linker groups,[63,64] we see no conductance features attributable to **CN** electrode-binding through the bridge N atoms. We suggest that such features are obscured by the primary conductance peak attributed to thioether connected junctions, or that the aryl groups in **CN** serve to sterically inhibit imidazole-electrode binding in these systems. Taken together, the most probable conductance values for the intact, thioether connected junctions, obtained from Gaussian fits to each peak in **Figure 2c**, are $G_{\mathbf{2CN}} = 5.3 \times 10^{-4}$ $G_0 \sim G_{\mathbf{CN}} = 4.3 \times 10^{-4}$ $G_0 > G_{\mathbf{BN}} = 2.4 \times 10^{-4}$ $G_0 > G_{\mathbf{BO}} = 8.7 \times 10^{-5}$ G_0.

From this first series of measurements, we recognize an apparent correlation between the decreasing conductance of molecules and the increasing $\Delta\chi$ between bridge group atoms.

Previous studies[39,65,66] (described in more detail below) have rationalized conductance trends within different molecular families in terms of the polarization of bridge bonds that serve to localize the molecular orbitals responsible for junction transport. To explore the potential impact of bond polarization in these DCC-bridged systems, we perform first-principles calculations to determine the electronic transmission of model molecular junctions comprising **2CN**, **CN**, **BN**, and **BO**. **Figure 2d** shows the transmission functions T(E) for these junctions, calculated using the DFT+Σ[61,62] approach within the NEGF formalism[47] (see "Computational Studies" in "Methods" section for technical details and the **SI, Table S1** for additional computational parameters). Reading T(E) at the Fermi level (E_F, set to be zero in **Figure 2d**), the computed conductance values are $G_{\mathbf{2CN}} = 7.7 \times 10^{-4}\ G_0 > G_{\mathbf{CN}} = 2.1 \times 10^{-4}\ G_0 > G_{\mathbf{BN}} = 1.9 \times 10^{-4}\ G_0 > G_{\mathbf{BO}} = 3.0 \times 10^{-5}\ G_0$. These values are in quantitative agreement with experimental results within a factor of 2 in general. From **Figure 2d**, for every junction, $T(E_F)$ is almost flat around E_F, being influenced by both a complex gateway state around -2 eV below E_F resulting from the hybridization between molecular orbitals and Au *d*-states and a well-defined lowest unoccupied molecular orbital (LUMO) resonance between 2-4 eV above E_F. The gateway states are similar in energy and shape for all junctions, hence we focus on the clear LUMO resonances in our analysis of the transmission differences for each junction. We note that the LUMO resonances exhibit a remarkable difference between the junctions with and without boron atoms. While the resonance peaks for **CN** and **2CN** (between 2-3 eV above E_F) approach unity, suggesting symmetric conducting orbitals, the resonance peaks for **BO** and **BN** (around 3 eV above E_F) are much smaller than 1, suggesting asymmetric conducting orbitals.[67] This difference indeed highlights the effect of the highly polarized B-O and B-N bonds (compared to the C-N bonds in **CN** and **2CN**) in trapping charges, making the molecular orbital asymmetric, and reducing their conductance in molecular junctions. Furthermore, **Figure 2e** shows the transmission eigenchannels[68] of **BN** and **BO** evaluated at their LUMO resonance peaks. The **BO** junction has a different nodal structure than that of **BN** and features charge localization around the oxygen atom (the lobes are not connected with lobes on other atoms), leading to an additional decrease in conductance compared to **BN**.

Beyond the interpretation of these molecular conductance trends, we also recognize that the histograms obtained from glovebox-based STM-BJ experiments presented in **Figure 2c** exhibit an apparent higher noise than for analogous measurements in air, as indicated by the increased counts between 10^{-2}-$10^{0}\ G_0$ and decreased resolution of atomic point contact features above ~1 G_0 (see also **SI, Figure S6**). While our glovebox STM-BJ setup operates in a more

challenging chemical, vibrational, and acoustic environment with the potential to increase measurement noise, we find that these apparent noise features are typically absent in clean gold measurements prior to the addition of solvent (see **SI, Figure S7a-c**, yellow). Glovebox STM-BJ studies in different anhydrous, deoxygenated solvents reveal that the apparent noise features are present when using TCB and mesitylene, but absent with tetradecane (TD; **SI, Figure S7a-c**, brown). We suggest that the observed "noise" results from increased interactions between aromatic solvent molecules and undercoordinated gold atoms during STM-BJ measurements in the absence of O_2 or H_2O. Additional discussion of these features is provided in the caption to **SI, Figure S7**.

Though they each comprise C-N bond motifs, the fact that **2CN** and **CN** junctions exhibit such comparable conductance is perhaps surprising given their different bridge connectivity (**Figure 2c**). The chemical structure of imidazole, diazaborole, and boronic ester bridges necessitates that one aryl group has bridge connections located at both *para* (1,4-) and *meta* (1,3-) positions relative to the thioether substituent in these model compounds. For phenylene bridges, such 1,3-substitution patterns are known to result in destructive interference effects that decrease junction conductance relative to their 1,4-substituted analogues.[69–71] While the two B-O/B-N bonds in **BO**/**BN** are formally identical, the imidazole bridge of **CN** contains distinct C-NH and C=N bonding motifs. Here the N-H proton can be transferred between nitrogen sites with a concurrent shift in the N=C double bond position via a tautomerization reaction,[72] formally positioning this either *para* (**CN-*p***) or *meta* (**CN-*m***) to the thioether substituent (**Figure 3a**). Indeed, the ^{1}H NMR spectrum of **CN** in DMSO-d_6 shows two distinguishable sets of resonances, indicating both tautomeric forms are present in DMSO solutions at room temperature (**SI, Figure S19**). However, we only observe one peak in the conductance histograms of **CN** measured in TCB (**Figure 2c**) or propylene carbonate (PC; **SI, Figure S9b**).

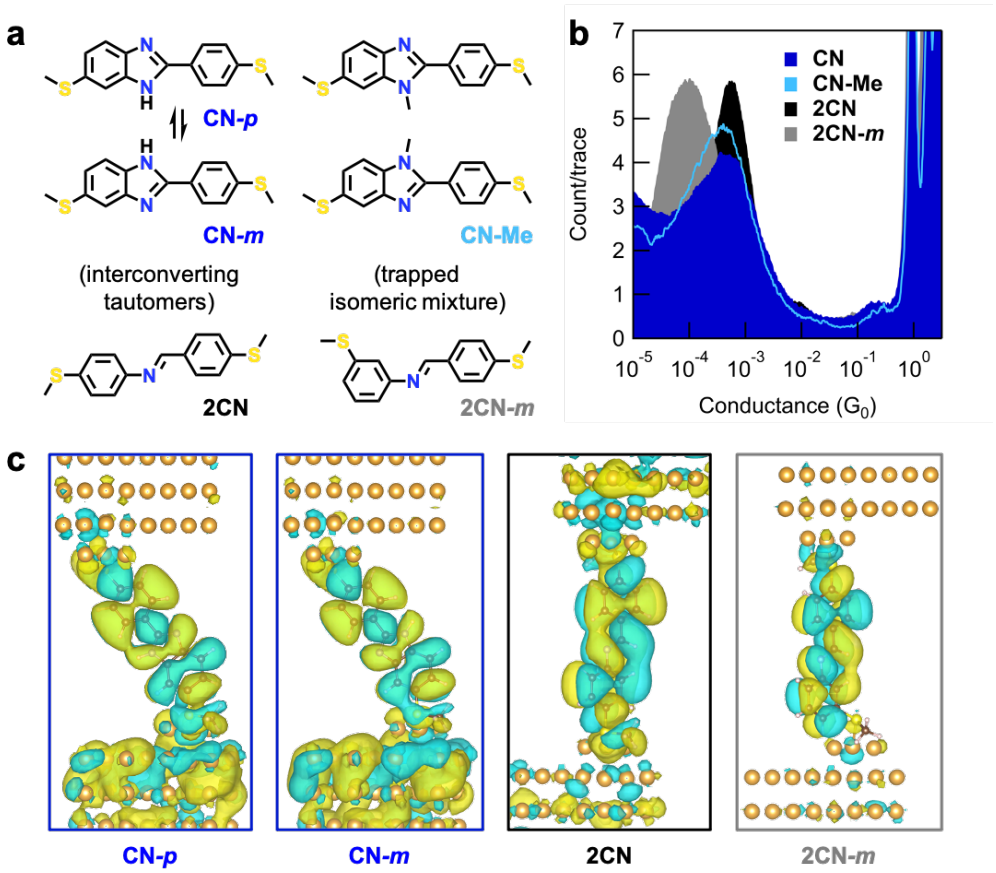

Figure 3. (a) Molecular structures of **CN** (now showing tautomeric equilibrium between **CN-*p*** and **CN-*m***), **CN-Me** (an isomeric mixture in ~1:1 ratio), **2CN**, and **2CN-*m***. **(b)** Overlaid 1D conductance histograms for **CN**, **CN-Me**, **2CN**, and **2CN-*m*** obtained in TCB (V_{bias} = 100 mV, 5,000-10,000 traces). **CN** and **CN-Me** junctions exhibit a single peak at comparable conductance, showing that the precise position of the C=N bond (and exchange of NH for N-Me) does not significantly change junction conductance. By comparison, **2CN-m**, a molecule with a *meta*-connected C=N linkage, has a conductance almost ~5 times lower than **2CN**. Histograms for **CN** and **2CN** are reproduced here from **Figure 2c** for convenience. **(c)** Transmission eigenchannels of the two tautomers of **CN**, **2CN**, and **2CN-*m***, evaluated at the LUMO resonance peaks. While the eigenchannels for **CN** tautomers are qualitatively similar, the eigenchannel for **2CN-*m*** shows an additional node and charge depletion at the thioether linker relative to **2CN** that leads to a lower conductance value.

To help rationalize these observations, we synthesize and study two additional control compounds: **CN-Me**, a ~1:1 mixture of each isomeric structure, trapped by replacing the readily exchanged N-H protons with inexchangable methyl groups; and **2CN-*m***, an analogue of **2CN** where the imine group is *meta*-connected to one of the thioether anchor groups (molecular structures provided in **Figure 3a**). In **Figure 3b**, we overlay conductance histograms for **CN**, **CN-Me**, **2CN**, and **2CN-*m***. Remarkably, measurements of the **CN-Me** mixture also show only a single conductance peak. As the peaks in **CN-Me** and **CN** histograms

occur at highly comparable conductance values, it is apparent that substitution of NH for NMe, and the formal position of the C=N double bond in **CN-Me** or **CN**, has only a minor impact on junction conductance (close to, or beyond, experimental resolution). In stark contrast, the most probable conductance of **2CN-*m*** junctions (9.7×10^{-5} G_0), with only a single C=N double bond *meta*-connected to the -SMe group, is ~5 times lower than for **2CN** junctions.

Such results are qualitatively supported by our first-principles calculations, where the difference between **2CN** and **2CN-*m*** is more pronounced than that between **CN-*p*** and **CN-*m***. The transmission functions for these junctions, calculated at the DFT+Σ level of theory, are shown in the **SI, Figure S12**. The sharp difference between the two conformations of **CN** and **2CN** is reflected in the transmission eigenchannel analysis (performed at the LUMO resonance peaks), shown in **Figure 3c**. While the eigenchannels for the two tautomers of **CN** are qualitatively similar, we observe different charge localization patterns near the linker thioether group between **2CN** and **2CN-*m***. In the case of **2CN-*m***, an additional node and charge depletion at the linker thioether group leads to a lower conductance value.

Our observations are also consistent with predictive chemical models. Application of the "extended curly arrow rules" recently presented by O'Driscoll and Bryce[73] to **CN-*m*** (where the C=N bond is positioned *meta* to -SMe, **Figure 3a**) suggest that it should exhibit a "*shifted* destructive" quantum interference (SDQI; **SI, Figure S8a**) rather than DQI. Here the electron-donating *para*-connected -NH- substituent (absent in **2CN-*m***) is considered to increase the conductance of this tautomer/isomer relative to that of **2CN-*m*** by moving the transmission antiresonance away from the Fermi level (E_F). While the predicted result from this model agrees with our findings for **CN-*m***, hybridization between molecular states and gold *d*-states complicates interpretation of the change in transmission in terms of a simple shift in antiresonance position (**SI, Figure S12**). We also note, for completeness, that further arrow pushing allows us to draw a zwitterionic resonance form for **CN-*m*** that places the C=N bond *para* to the -SMe group (**SI, Figure S8b**), resulting in an electronic structure that resembles that of the most important resonance form of **CN-*p***.

To explore how bridge group composition influences through-bond transport in extended materials, we next study a series of analogous compounds comprising two bridge groups (**2CN-L**, **CN-L**, **BN-L**, and **BO-L**; **Figure 4a**). **BO-L**, containing easily hydrolyzed boronic ester groups, was again measured under an inert atmosphere in the glovebox (now using V_{bias} = 750 mV to lower the instrumental noise floor and better resolve the conductance peak). **BN-L** was measured as a PC solution (in air) due to the poor solubility of this compound in TCB. Control studies of **2CN**, **2CN-L**, **CN**, **CN-L**, **BN**, and **BN-L** in PC show that changes

in solvent or bias polarity (at low biases) do not significantly impact the most probable conductance of their molecular junctions (**SI, Figure S9**). These experiments further support our computational studies which show T(E) is almost flat around E_F (little to no current rectification should be observed when opening the bias window asymmetrically in polar solvents;[74] **Figure 2d** and **SI, Figure 13**), and show it is reasonable to directly compare the conductance of **BN-L** in PC with the conductance of other molecules measured in TCB. In **Figure 4b**, we present overlaid 1D conductance histograms for this longer series of molecules. Their conductance broadly exhibits the same correlation with bridge composition as observed for the shorter series, with $G_{\mathbf{2CN\text{-}L}} = 9.8 \times 10^{-5}\ G_0 > G_{\mathbf{CN\text{-}L}} = 4.6 \times 10^{-5}\ G_0 > G_{\mathbf{BN\text{-}L}} = 2.4 \times 10^{-5}\ G_0 > G_{\mathbf{BO\text{-}L}} = 3.0 \times 10^{-6}\ G_0$. The same trend is predicted from our first-principles NEGF calculations using DFT+Σ: $G_{\mathbf{2CN\text{-}L}} = 1.9 \times 10^{-4}\ G_0 > G_{\mathbf{CN\text{-}L}} = 1.6 \times 10^{-4}\ G_0 > G_{\mathbf{BN\text{-}L}} = 8.6 \times 10^{-6}\ G_0 > G_{\mathbf{BO\text{-}L}} = 3.8 \times 10^{-6}\ G_0$ (transmission functions are shown in the **SI, Figure S13**). Transmission eigenchannel analysis carried out at the LUMO resonance peaks for the longer molecules (**SI, Figure S14**) shows that the LUMO resonance is symmetric for all molecules (their structures exhibit C_2-symmetry about the central aromatic ring, as drawn in **Figure 4a**). As a result, in contrast to observations for **BN** and **BO** (**Figure 2d**), T(E) for **BN-L** and **BO-L** now reaches unity between 2-3 eV above E_F (**SI, Figure S13**). The LUMO resonances for the long boron-containing molecules are noticeably narrower than for those without boron atoms (indicating reduced electronic coupling to the electrodes) and the resonance for **BO-L** shows distinct charge localization near the oxygen atoms, consistent with our findings for the short molecules (**Figure 2e)**.

In **Figure 4c** and **4d**, respectively, we summarize our findings by plotting the measured and computed conductance against the number of DCC groups. However, we emphasize that these values cannot be used to determine true tunneling decay constants (β-values). Due to synthetic challenges, we compare structures without exact oligomeric repeating groups and only isolate and study molecules of two lengths. As an alternative metric for tunneling decay, we instead calculate the ratio of conductance for molecules with 1 and 2 bridge groups for each series ($G_{1/2}$). We find the largest measured conductance ratio is $G_{\mathbf{BO/BO\text{-}L}} = 28.6$ ($G_{\mathbf{2CN/2CN\text{-}L}} = 5.42$, $G_{\mathbf{CN/CN\text{-}L}} = 9.2$, $G_{\mathbf{BN/BN\text{-}L}} = 9.9$), showing that addition of a second boronic ester group most significantly impacts the conductance of junctions compared to the other DCC bridge types studied. The conductance ratios for $G_{\mathbf{CN/BO}}$ (one bridge group) and $G_{\mathbf{CN\text{-}L/BO\text{-}L}}$ (two bridge groups) junctions are ~6 and ~33, respectively, further highlighting the potential cumulative impact of bridge choice on transport processes in extended systems.

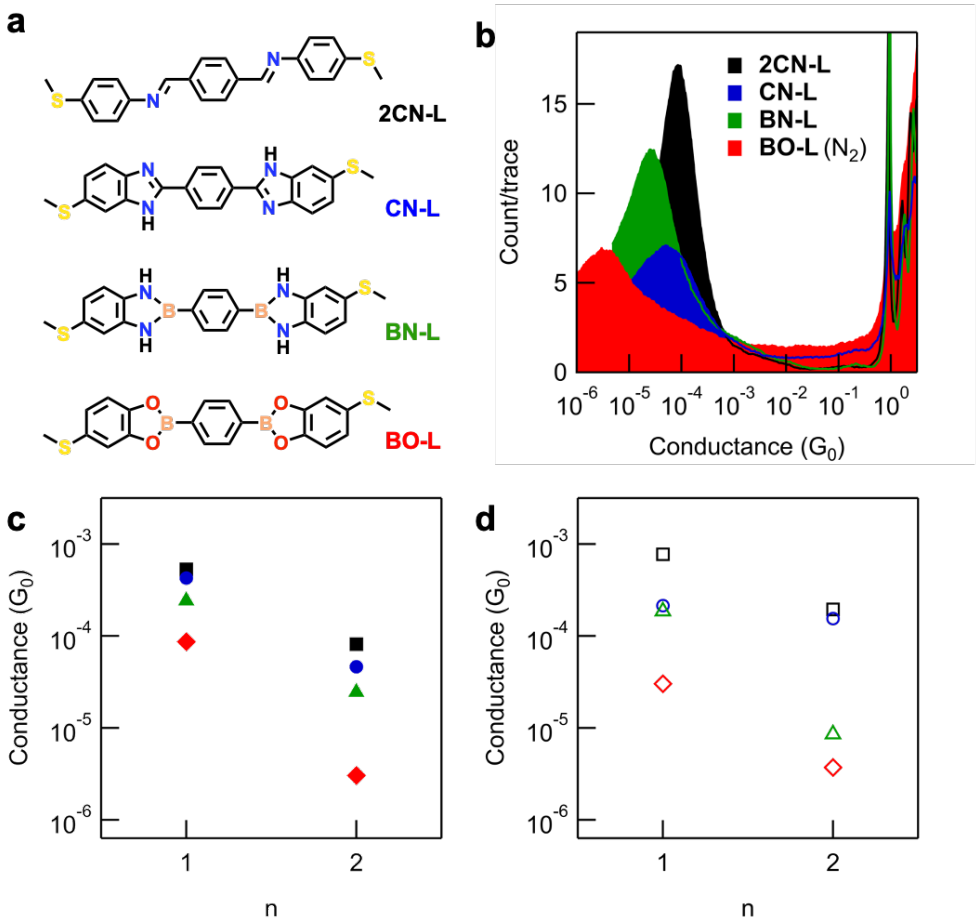

Figure 4. (a) Molecular structures of model compounds containing two DCC bridge groups. **CN-L** has three tautomeric forms but is drawn here with both C=N bonds *para* to terminal thioether groups for simplicity. **(b)** Overlaid 1D conductance histograms for junctions comprising two DCC bridge groups (10,000 traces). **BO-L** (red) is measured in TCB under an inert nitrogen atmosphere with V_{bias} = 750 mV. All other molecules are measured in TCB in air with V_{bias} = 100 mV, except for **BN-L** (green) which is measured in PC in air (V_{bias} = +100 mV, applied to the tip). **(c)** A plot of measured conductance versus number of bridge groups (n), showing that junction conductance decays more rapidly with length extension in systems containing boronic esters (red) compared to other bridges. Conductance values were obtained from Gaussian fits to peaks in histograms presented here and in **Figure 2c**. **(d)** The same plot as (c), but for calculated conductance from DFT+Σ. This illustrates the same qualitative trends.

From **Figure 4c** and **4d**, we clearly see a general correlation between the decreasing conductance of molecules with different DCC bridges, $G_{2C\text{-}N} \gtrsim G_{C\text{-}N} > G_{B\text{-}N} > G_{B\text{-}O}$, and the increasing $\Delta\chi$ between bridge group atoms. As noted above, bond polarization resulting from the $\Delta\chi$ of bridge atoms has been used to rationalize the low conductance of oligosiloxanes[39] ($\Delta\chi_{(Si\text{-}O)}$ = 1.54) and peptides[65] ($\Delta\chi_{(C\text{-}N)}$ = 0.49), compared to alkanethiols of similar length ($\Delta\chi_{(C\text{-}C)}$ = 0). A related study of fluorene-based wires, with methylene bridges replaced by different groups, found that a NPh-bridge provided a higher conductance system than an O-

bridge.[66] This result was attributed to the higher energy (lower χ) filled p-orbital of the sp^2 hybridized N atom, improving alignment and orbital overlap with the carbon-based π-system. Similar arguments have been applied to interpret the properties of 2D COFs comprising 1,3,5-connected benzene or analogous triazine and boroxine rings.[75] Decreased π-conjugation is thought to contribute to larger band gaps and reduced band dispersion.

For the compounds studied here the B-O bonds of the boronic ester groups are the most ionic in character, resulting from energetically well-separated B and O sp^2 hybrid atomic orbitals. While it may be considered that the B-O and B-N bonds in boronic esters and diazaboroles exhibit partial double bond character due to donation from O/N lone pairs to the empty B p_z orbital, the extent of π-conjugation is again expected to be reduced for B-O compared to B-N systems in line with their $\Delta\chi$.[76] This further helps to rationalize the increased conductance of **BN**/**BN-L** junctions compared to **BO**/**BO-L**. These heuristic arguments are further supported by the transmission eigenchannel analysis (**Figure 2e** and **Figure 3c**). To be specific, the polarized bonds between B-N and B-O introduce local asymmetry into the molecular orbital, which makes the resonance peak corresponding to the LUMO much lower than 1, or significantly decreases its coupling to the electrode (**Figure 2d** and **SI, Figure S13**). These effects decrease the conductance values for the boron-containing species compared to others. Moreover, the oxygen atoms introduce additional charge localization and a different nodal structure in the transmission eigenchannels, making the B-O containing species least conductive.

CONCLUSIONS

This work underscores an emerging dimensional reduction strategy to probe the intrinsic electronic structure of molecule-based porous extended materials from the bottom up, by studying charge transport through atomically precise molecular junctions comprising appropriate model compounds ("framework fragments"). Specifically, we have shown that it is possible to resolve, quantify, and rationalize conductance differences for fragments comprising 1 or 2 DCC bridge groups of similar connectivity but distinct composition. We find that imine bridges are the most, and polarized boronic ester bridges the least, electronically transparent to tunnelling electrons in 1D. It is our hope that this and related investigations will provide new perspectives on electronic transport in COFs and MOFs that not only complement existing characterization techniques, but also serve to help inspire new advances in material properties and capabilities.

Development of a robust glovebox-based STM-BJ setup proved critical for studying molecules comprising boronic esters that appear to hydrolyze when measured in air. Control experiments show that the rigorous exclusion of O_2 or H_2O does not significantly change the conductance of the intact molecular junctions studied but does appear to complicate measurements performed using gold electrodes in aromatic solvents. Though further establishing studies are needed, we anticipate that such rigorously air-free STM-BJ systems will provide access to a greatly expanded scope of ambient-pressure single-molecule junction experiments involving air-sensitive molecular backbones, linkers, and/or electrode materials with the potential to expose a suite of unusual nanoscale chemical and charge transport phenomena.

EXPERIMENTAL SECTION

Conductance Measurements

We apply the STM-BJ method in air, and under an inert atmosphere in an anhydrous, nitrogen-filled glovebox, to measure the conductance of single-molecule junctions using custom-built instrumentation described in detail elsewhere and in the **SI**.[54,77,78] Briefly, we apply a bias voltage (V_{bias}) across a mechanically cut gold STM tip and thin film gold substrate, and measure the current (I) as these electrodes are repeatedly pushed in and out of electrical contact. With increasing tip-substrate displacement, the initially formed metallic junction thins to a single atom point contact with a conductance ($G = I/V_{bias}$) close to 1 G_0 ($= 2e^2/h = 7.748 \times 10^{-5}$ S). With continued tip retraction the point contact breaks to form nanogap separated electrodes. In the presence of molecules that can bridge the gap, we form gold-molecule-gold junctions as indicated by the observation of new step features below 1 G_0 in conductance-displacement traces. We construct 1D and 2D histograms without data selection from thousands of consecutively measured conductance-displacement traces for statistical analysis. Unless otherwise stated, data is obtained using 0.1-1 mM analyte solutions in TCB that have been prepared and measured in air.

Computational Studies

The junction structures were constructed by placing seven Au (111) layers (with 4×4 Au atoms on each layer) at each side of the molecule, with the sulfur atom in the molecule binding to an Au trimer.[79,80] During the geometry relaxation, the outer three Au layers on each side were considered as a rigid body, with their relative positions kept as those in the bulk and the force acting on these three Au layers taken as the average force on the atoms in the fourth Au layer.

All degrees of freedom of the extended molecule (the inner three Au layers on each side + an Au trimer on each side + the molecule) are fully relaxed, until all forces are below 0.04 eV/Å. The geometry relaxation used the SIESTA package,[81] the Perdew-Burke-Ernzerhof (PBE) functional,[82] a 4×4×1 k-mesh. The Au pseudopotential and basis functions were adapted from prior work[61] and were chosen to reproduce the work function of Au (111) surface. Single-zeta basis functions were used for Au, and double-zeta basis functions were used for all other elements.

After junction geometry relaxation, the transport calculations were performed within the framework of non-equilibrium Green's function as implemented in TranSIESTA,[47] using the same functional, pseudopotential, basis set, and k-point sampling. After the non-equilibrium density matrix is converged, the coherent transmission functions as a function of energy were computed using the Landauer formula in a post-processing manner,[83] with a 16×16 k-mesh. To correct the quantitative errors of PBE functional in estimating the transport properties, the DFT+Σ approach[61,62] was applied following the procedure outlined by Liu *et al.*[79] The detailed computational parameters for the DFT+Σ calculations are reported in the Supporting Information.

ASSOCIATED CONTENT

Electronic Supplementary Information (ESI) available: Additional synthetic, STM-BJ, and computational details, synthetic procedures, 1D and 2D conductance histograms, transmission calculations, ^{1}H and ^{13}C{^{1}H} NMR spectra for all new compounds.

AUTHOR INFORMATION

Corresponding Author

Zhen-Fei Liu – Email: zfliu@wayne.edu
Michael S. Inkpen – Email: inkpen@usc.edu

Notes

The authors declare no competing financial interest.

ACKNOWLEDGEMENTS

Experimental work was primarily supported by University of Southern California (USC) startup funds. M.S.I. thanks E-Dean Fung, Tianren Fu, and Latha Venkataraman for assistance with construction of air-based STM-BJ instrumentation, and Sully Chen for help with system calibration. N.R. was supported by a Marie Skłodowska Curie Global Fellowship (HOPELEC:

898657) within the Horizon 2020 Programme. J.M.P. is grateful for additional support from a USC Wrigley Institute for Environmental Studies Norma and Jerol Sonosky Environmental Sustainability Graduate Summer Fellowship. Z.-F.L. acknowledges support from the NSF for a CAREER award, DMR-2044552. We thank the NSF (DBI-0821671, CHE-0840366, CHE-1048807) and the NIH (S10 RR25432) for analytical instrumentation.

REFERENCES

(1) Yaghi, O. M.; Kalmutzki, M. J.; Diercks, C. S. *Introduction to Reticular Chemistry: Metal-Organic Frameworks and Covalent Organic Frameworks*, 1st ed.; Wiley Online Books; Wiley-VCH Verlag GmbH & Co. KGaA: Weinheim, Germany, 2019.

(2) Ma, T.; Kapustin, E. A.; Yin, S. X.; Liang, L.; Zhou, Z.; Niu, J.; Li, L.-H.; Wang, Y.; Su, J.; Li, J.; Wang, X.; Wang, W. D.; Wang, W.; Sun, J.; Yaghi, O. M. Single-Crystal X-Ray Diffraction Structures of Covalent Organic Frameworks. *Science* **2018**, *361*, 48–52.

(3) Haase, F.; Lotsch, B. V. Solving the COF Trilemma: Towards Crystalline, Stable and Functional Covalent Organic Frameworks. *Chem. Soc. Rev.* **2020**, *49*, 8469–8500.

(4) Yan, Y.; He, T.; Zhao, B.; Qi, K.; Liu, H.; Xia, B. Y. Metal/Covalent-Organic Frameworks-Based Electrocatalysts for Water Splitting. *J. Mater. Chem. A* **2018**, *6*, 15905–15926.

(5) Downes, C. A.; Marinescu, S. C. Electrocatalytic Metal–Organic Frameworks for Energy Applications. *ChemSusChem* **2017**, *10*, 4374–4392.

(6) Kreno, L. E.; Leong, K.; Farha, O. K.; Allendorf, M.; Van Duyne, R. P.; Hupp, J. T. Metal–Organic Framework Materials as Chemical Sensors. *Chem. Rev.* **2012**, *112*, 1105–1125.

(7) Meng, Z.; Stolz, R. M.; Mendecki, L.; Mirica, K. A. Electrically-Transduced Chemical Sensors Based on Two-Dimensional Nanomaterials. *Chem. Rev.* **2019**, *119*, 478–598.

(8) Zhang, Y.; Riduan, S. N.; Wang, J. Redox Active Metal- and Covalent Organic Frameworks for Energy Storage: Balancing Porosity and Electrical Conductivity. *Chem. - A Eur. J.* **2017**, *23*, 16419–16431.

(9) Xiao, X.; Zou, L.; Pang, H.; Xu, Q. Synthesis of Micro/Nanoscaled Metal-Organic Frameworks and Their Direct Electrochemical Applications. *Chem. Soc. Rev.* **2020**, *49*, 301–331.

(10) Gao, H.; Shen, H.; Wu, H.; Jing, H.; Sun, Y.; Liu, B.; Chen, Z.; Song, J.; Lu, L.; Wu, Z.; Hao, Q. Review of Pristine Metal-Organic Frameworks for Supercapacitors: Recent Progress and Perspectives. *Energy and Fuels* **2021**, *35*, 12884–12901.

(11) Miner, E. M.; Dincă, M. Metal- and Covalent-Organic Frameworks as Solid-State Electrolytes for Metal-Ion Batteries. *Philos. Trans. R. Soc. A Math. Phys. Eng. Sci.* **2019**, *377*, 20180225.

(12) Calbo, J.; Golomb, M. J.; Walsh, A. Redox-Active Metal–Organic Frameworks for Energy Conversion and Storage. *J. Mater. Chem. A* **2019**, *7*, 16571–16597.

(13) Sun, L.; Campbell, M. G.; Dincă, M. Electrically Conductive Porous Metal–Organic Frameworks. *Angew. Chem. Int. Ed.* **2016**, *55*, 3566–3579.

(14) Aubrey, M. L.; Wiers, B. M.; Andrews, S. C.; Sakurai, T.; Reyes-Lillo, S. E.; Hamed, S. M.; Yu, C.-J.; Darago, L. E.; Mason, J. A.; Baeg, J.-O.; Grandjean, F.; Long, G. J.; Seki, S.; Neaton, J. B.; Yang, P.; Long, J. R. Electron Delocalization and Charge Mobility as a Function of Reduction in a Metal–Organic Framework. *Nat. Mater.* **2018**, *17*, 625–632.

(15) Day, R. W.; Bediako, D. K.; Rezaee, M.; Parent, L. R.; Skorupskii, G.; Arguilla, M. Q.; Hendon, C. H.; Stassen, I.; Gianneschi, N. C.; Kim, P.; Dincă, M. Single Crystals of Electrically Conductive Two-Dimensional Metal–Organic Frameworks: Structural and Electrical Transport Properties. *ACS Cent. Sci.* **2019**, *5*, 1959–1964.
(16) Dou, J.; Arguilla, M. Q.; Luo, Y.; Li, J.; Zhang, W.; Sun, L.; Mancuso, J. L.; Yang, L.; Chen, T.; Parent, L. R.; Skorupskii, G.; Libretto, N. J.; Sun, C.; Yang, M. C.; Dip, P. V.; Brignole, E. J.; Miller, J. T.; Kong, J.; Hendon, C. H.; Sun, J.; Dincă, M. Atomically Precise Single-Crystal Structures of Electrically Conducting 2D Metal–Organic Frameworks. *Nat. Mater.* **2021**, *20*, 222–228.
(17) Xie, L. S.; Skorupskii, G.; Dincă, M. Electrically Conductive Metal–Organic Frameworks. *Chem. Rev.* **2020**, *120*, 8536–8580.
(18) Souto, M.; Perepichka, D. F. Electrically Conductive Covalent Organic Frameworks: Bridging the Fields of Organic Metals and 2D Materials. *J. Mater. Chem. C* **2021**, *9*, 10668–10676.
(19) Wan, S.; Gándara, F.; Asano, A.; Furukawa, H.; Saeki, A.; Dey, S. K.; Liao, L.; Ambrogio, M. W.; Botros, Y. Y.; Duan, X.; Seki, S.; Stoddart, J. F.; Yaghi, O. M. Covalent Organic Frameworks with High Charge Carrier Mobility. *Chem. Mater.* **2011**, *23*, 4094–4097.
(20) Long, J. R.; Williamson, A. S.; Holm, R. H. Dimensional Reduction of $Re_6Se_8Cl_2$: Sheets, Chains, and Discrete Clusters Composed of Chloride-Terminated $[Re_6Q_8]^{2+}$ (Q = S, Se) Cores. *Angew. Chem. Int. Ed.* **1995**, *34*, 226–229.
(21) Tulsky, E. G.; Long, J. R. Dimensional Reduction: A Practical Formalism for Manipulating Solid Structures. *Chem. Mater.* **2001**, *13*, 1149–1166.
(22) Smith, M. K.; Northrop, B. H. Vibrational Properties of Boroxine Anhydride and Boronate Ester Materials: Model Systems for the Diagnostic Characterization of Covalent Organic Frameworks. *Chem. Mater.* **2014**, *26*, 3781–3795.
(23) Zwaneveld, N. A. A.; Pawlak, R.; Abel, M.; Catalin, D.; Gigmes, D.; Bertin, D.; Porte, L. Organized Formation of 2D Extended Covalent Organic Frameworks at Surfaces. *J. Am. Chem. Soc.* **2008**, *130*, 6678–6679.
(24) Chen, C.; Joshi, T.; Li, H.; Chavez, A. D.; Pedramrazi, Z.; Liu, P.-N.; Li, H.; Dichtel, W. R.; Bredas, J.-L.; Crommie, M. F. Local Electronic Structure of a Single-Layer Porphyrin-Containing Covalent Organic Framework. *ACS Nano* **2018**, *12*, 385–391.
(25) Yang, L.; He, X.; Dincă, M. Triphenylene-Bridged Trinuclear Complexes of Cu: Models for Spin Interactions in Two-Dimensional Electrically Conductive Metal-Organic Frameworks. *J. Am. Chem. Soc.* **2019**, *141*, 10475–10480.
(26) Intrator, J. A.; Orchanian, N. M.; Clough, A. J.; Haiges, R.; Marinescu, S. C. Electronically-Coupled Redox Centers in Trimetallic Cobalt Complexes. *Dalton Trans.* **2022**, *51*, 5660–5672.
(27) Zasada, L. B.; Guio, L.; Kamin, A. A.; Dhakal, D.; Monahan, M.; Seidler, G. T.; Luscombe, C. K.; Xiao, D. J. Conjugated Metal–Organic Macrocycles: Synthesis, Characterization, and Electrical Conductivity. *J. Am. Chem. Soc.* **2022**, *144*, 4515–4521.
(28) Murase, R.; Leong, C. F.; D'Alessandro, D. M. Mixed Valency as a Strategy for Achieving Charge Delocalization in Semiconducting and Conducting Framework Materials. *Inorg. Chem.* **2017**, *56*, 14373–14382.
(29) Lin, S.; Usov, P. M.; Morris, A. J. The Role of Redox Hopping in Metal-Organic Framework Electrocatalysis. *Chem. Commun.* **2018**, *54*, 6965–6974.
(30) Wan, S.; Guo, J.; Kim, J.; Ihee, H.; Jiang, D. A Belt-Shaped, Blue Luminescent, and Semiconducting Covalent Organic Framework. *Angew. Chem. Int. Ed.* **2008**, *47*, 8826–8830.

(31) Narayan, T. C.; Miyakai, T.; Seki, S.; Dincă, M. High Charge Mobility in a Tetrathiafulvalene-Based Microporous Metal-Organic Framework. *J. Am. Chem. Soc.* **2012**, *134*, 12932–12935.
(32) Clough, A. J.; Skelton, J. M.; Downes, C. A.; de la Rosa, A. A.; Yoo, J. W.; Walsh, A.; Melot, B. C.; Marinescu, S. C. Metallic Conductivity in a Two-Dimensional Cobalt Dithiolene Metal–Organic Framework. *J. Am. Chem. Soc.* **2017**, *139*, 10863–10867.
(33) Skorupskii, G.; Trump, B. A.; Kasel, T. W.; Brown, C. M.; Hendon, C. H.; Dincă, M. Efficient and Tunable One-Dimensional Charge Transport in Layered Lanthanide Metal–Organic Frameworks. *Nat. Chem.* **2020**, *12*, 131–136.
(34) Gutzler, R.; Perepichka, D. F. Π-Electron Conjugation in Two Dimensions. *J. Am. Chem. Soc.* **2013**, *135*, 16585–16594.
(35) Thomas, S.; Li, H.; Zhong, C.; Matsumoto, M.; Dichtel, W. R.; Bredas, J.-L. Electronic Structure of Two-Dimensional π-Conjugated Covalent Organic Frameworks. *Chem. Mater.* **2019**, *31*, 3051–3065.
(36) Ni, X.; Brédas, J. L. Electronic Structure of Zinc-5,10,15,20-Tetraethynylporphyrin: Evolution from the Molecule to a One-Dimensional Chain, a Two-Dimensional Covalent Organic Framework, and a Nanotube. *Chem. Mater.* **2022**, *34*, 1334–1341.
(37) Ni, X.; Li, H.; Liu, F.; Brédas, J. L. Engineering of Flat Bands and Dirac Bands in Two-Dimensional Covalent Organic Frameworks (COFs): Relationships among Molecular Orbital Symmetry, Lattice Symmetry, and Electronic-Structure Characteristics. *Mater. Horizons* **2022**, *9*, 88–98.
(38) Hoffmann, R. How Chemistry and Physics Meet in the Solid State. *Angew. Chem. Int. Ed.* **1987**, *26*, 846–878.
(39) Li, H.; Garner, M. H.; Su, T. A.; Jensen, A.; Inkpen, M. S.; Steigerwald, M. L.; Venkataraman, L.; Solomon, G. C.; Nuckolls, C. Extreme Conductance Suppression in Molecular Siloxanes. *J. Am. Chem. Soc.* **2017**, *139*, 10212–10215.
(40) Low, J. Z.; Sanders, S. N.; Campos, L. M. Correlating Structure and Function in Organic Electronics: From Single Molecule Transport to Singlet Fission. *Chem. Mater.* **2015**, *27*, 5453–5463.
(41) Palomino-Ruiz, L.; Rodríguez-González, S.; Fallaque, J. G.; Márquez, I. R.; Agraït, N.; Díaz, C.; Leary, E.; Cuerva, J. M.; Campaña, A. G.; Martín, F.; Millán, A.; González, M. T. Single-Molecule Conductance of 1,4-Azaborine Derivatives as Models of BN-Doped PAHs. *Angew. Chem. Int. Ed.* **2021**, *60*, 6609–6616.
(42) Vladyka, A.; Perrin, M. L.; Overbeck, J.; Ferradás, R. R.; García-Suárez, V.; Gantenbein, M.; Brunner, J.; Mayor, M.; Ferrer, J.; Calame, M. In-Situ Formation of One-Dimensional Coordination Polymers in Molecular Junctions. *Nat. Commun.* **2019**, *10*, 262.
(43) Uribe-Romo, F. J.; Hunt, J. R.; Furukawa, H.; Klöck, C.; O'Keeffe, M.; Yaghi, O. M. A Crystalline Imine-Linked 3-D Porous Covalent Organic Framework. *J. Am. Chem. Soc.* **2009**, *131*, 4570–4571.
(44) Ranjeesh, K. C.; Illathvalappil, R.; Veer, S. D.; Peter, J.; Wakchaure, V. C.; Goudappagouda; Raj, K. V.; Kurungot, S.; Babu, S. S. Imidazole-Linked Crystalline Two-Dimensional Polymer with Ultrahigh Proton-Conductivity. *J. Am. Chem. Soc.* **2019**, *141*, 14950–14954.
(45) Kahveci, Z.; Sekizkardes, A. K.; Arvapally, R. K.; Wilder, L.; El-Kaderi, H. M. Highly Porous Photoluminescent Diazaborole-Linked Polymers: Synthesis, Characterization, and Application to Selective Gas Adsorption. *Polym. Chem.* **2017**, *8*, 2509–2515.
(46) Côté, A. P.; Benin, A. I.; Ockwig, N. W.; O'Keeffe, M.; Matzger, A. J.; Yaghi, O. M. Porous, Crystalline, Covalent Organic Frameworks. *Science* **2005**, *310*, 1166–1170.

(47) Brandbyge, M.; Mozos, J.-L.; Ordejón, P.; Taylor, J.; Stokbro, K. Density-Functional Method for Nonequilibrium Electron Transport. *Phys. Rev. B* **2002**, *65*, 165401.
(48) Park, Y. S.; Whalley, A. C.; Kamenetska, M.; Steigerwald, M. L.; Hybertsen, M. S.; Nuckolls, C.; Venkataraman, L. Contact Chemistry and Single-Molecule Conductance: A Comparison of Phosphines, Methyl Sulfides, and Amines. *J. Am. Chem. Soc.* **2007**, *129*, 15768–15769.
(49) Park, Y. S.; Widawsky, J. R.; Kamenetska, M.; Steigerwald, M. L.; Hybertsen, M. S.; Nuckolls, C.; Venkataraman, L. Frustrated Rotations in Single-Molecule Junctions. *J. Am. Chem. Soc.* **2009**, *131*, 10820–10821.
(50) Kabalka, G. W.; Reddy, N. K.; Narayana, C. Sodium Percarbonate: A Convenient Reagent for the Dakin Reaction. *Tetrahedron Lett.* **1992**, *33*, 865–866.
(51) Yanson, A. I.; Rubio Bollinger, G.; Van Den Brom, H. E.; Agraït, N.; Van Ruitenbeek, J. M. Formation and Manipulation of a Metallic Wire of Single Gold Atoms. *Nature* **1998**, *395*, 783–785.
(52) Quek, S. Y.; Kamenetska, M.; Steigerwald, M. L.; Choi, H. J.; Louie, S. G.; Hybertsen, M. S.; Neaton, J. B.; Venkataraman, L. Mechanically Controlled Binary Conductance Switching of a Single-Molecule Junction. *Nat. Nanotechnol.* **2009**, *4*, 230–234.
(53) Hong, W.; Manrique, D. Z.; Moreno-García, P.; Gulcur, M.; Mishchenko, A.; Lambert, C. J.; Bryce, M. R.; Wandlowski, T. Single Molecular Conductance of Tolanes: Experimental and Theoretical Study on the Junction Evolution Dependent on the Anchoring Group. *J. Am. Chem. Soc.* **2011**, *134*, 2292–2304.
(54) Venkataraman, L.; Klare, J. E.; Tam, I. W.; Nuckolls, C.; Hybertsen, M. S.; Steigerwald, M. L. Single-Molecule Circuits with Well-Defined Molecular Conductance. *Nano Lett.* **2006**, *6*, 458–462.
(55) Olavarría-Contreras, I. J.; Etcheverry-Berríos, A.; Qian, W.; Gutiérrez-Cerón, C.; Campos-Olguín, A.; Sañudo, E. C.; Dulić, D.; Ruiz, E.; Aliaga-Alcalde, N.; Soler, M.; Van Der Zant, H. S. J. Electric-Field Induced Bistability in Single-Molecule Conductance Measurements for Boron Coordinated Curcuminoid Compounds. *Chem. Sci.* **2018**, *9*, 6988–6996.
(56) Liu, X.; Li, X.; Sangtarash, S.; Sadeghi, H.; Decurtins, S.; Häner, R.; Hong, W.; Lambert, C. J.; Liu, S. X. Probing Lewis Acid-Base Interactions in Single-Molecule Junctions. *Nanoscale* **2018**, *10*, 18131–18134.
(57) Zhao, Z.-H.; Wang, L.; Li, S.; Zhang, W.-D.; He, G.; Wang, D.; Hou, S.-M.; Wan, L.-J. Single-Molecule Conductance through an Isoelectronic B–N Substituted Phenanthrene Junction. *J. Am. Chem. Soc.* **2020**, *142*, 8068–8073.
(58) Zhao, Y.-Q.; Lan, J.-Q.; Hu, C.-E.; Mu, Y.; Chen, X.-R. Electron Transport of the Nanojunctions of (BN) n (n = 1–4) Linear Chains: A First-Principles Study. *ACS Omega* **2021**, *6*, 15727–15736.
(59) Baghernejad, M.; Van Dyck, C.; Bergfield, J.; Levine, D. R.; Gubicza, A.; Tovar, J. D.; Calame, M.; Broekmann, P.; Hong, W. Quantum Interference Enhanced Chemical Responsivity in Single-Molecule Dithienoborepin Junctions. *Chem. - A Eur. J.* **2019**, *25*, 15141–15146.
(60) Li, H.; Wang, R.; Song, K.; Wei, C.; Hong, W.; Zang, Y.; Qu, D. Substitution Pattern Controlled Charge Transport in BN-Embedded Aromatics-Based Single-Molecule Junctions. *Phys. Chem. Chem. Phys.* **2022**, *24*, 2227–2233.
(61) Quek, S. Y.; Venkataraman, L.; Choi, H. J.; Louie, S. G.; Hybertsen, M. S.; Neaton, J. B. Amine−Gold Linked Single-Molecule Circuits: Experiment and Theory. *Nano Lett.* **2007**, *7*, 3477–3482.
(62) Neaton, J. B.; Hybertsen, M. S.; Louie, S. G. Renormalization of Molecular Electronic

Levels at Metal-Molecule Interfaces. *Phys. Rev. Lett.* **2006**, *97*, 216405.
(63) Fu, T.; Smith, S.; Camarasa-Gómez, M.; Yu, X.; Xue, J.; Nuckolls, C.; Evers, F.; Venkataraman, L.; Wei, S. Enhanced Coupling through π-Stacking in Imidazole-Based Molecular Junctions. *Chem. Sci.* **2019**, *10*, 9998–10002.
(64) Pan, X.; Lawson, B.; Rustad, A.; Kamenetska, M. PH-Activated Single Molecule Conductance and Binding Mechanism of Imidazole on Gold. *Nano Lett.* **2020**, *20*, 4687–4692.
(65) Brisendine, J. M.; Refaely-Abramson, S.; Liu, Z.-F.; Cui, J.; Ng, F.; Neaton, J. B.; Koder, R. L.; Venkataraman, L. Probing Charge Transport through Peptide Bonds. *J. Phys. Chem. Lett.* **2018**, *9*, 763–767.
(66) Klausen, R. S.; Widawsky, J. R.; Su, T. A.; Li, H.; Chen, Q.; Steigerwald, M. L.; Venkataraman, L.; Nuckolls, C. Evaluating Atomic Components in Fluorene Wires. *Chem. Sci.* **2014**, *5*, 1561–1564.
(67) Liu, Z. F.; Neaton, J. B. Voltage Dependence of Molecule-Electrode Coupling in Biased Molecular Junctions. *J. Phys. Chem. C* **2017**, *121*, 21136–21144.
(68) Paulsson, M.; Brandbyge, M. Transmission Eigenchannels from Nonequilibrium Green's Functions. *Phys. Rev. B* **2007**, *76*, 115117.
(69) Sautet, P.; Joachim, C. Electronic Interference Produced by a Benzene Embedded in a Polyacetylene Chain. *Chem. Phys. Lett.* **1988**, *153*, 511–516.
(70) Mayor, M.; Weber, H. B.; Reichert, J.; Elbing, M.; von Hanisch, C.; Beckmann, D.; Fisher, M. Electric Current through a Molecular Rod - Relevance of the Position of the Anchor Groups. *Angew. Chem., Int. Ed. Engl.* **2003**, *42*, 5834–5838.
(71) Solomon, G. C.; Herrmann, C.; Hansen, T.; Mujica, V.; Ratner, M. A. Exploring Local Currents in Molecular Junctions. *Nat. Chem.* **2010**, *2*, 223–228.
(72) Khristich, B. I. Tautomerism in a Number of Asymmetrical Imidazole Systems. *Chem. Heterocycl. Compd.* **1970**, *6*, 1572–1575.
(73) O'Driscoll, L. J.; Bryce, M. R. Extended Curly Arrow Rules to Rationalise and Predict Structural Effects on Quantum Interference in Molecular Junctions. *Nanoscale* **2021**, *13*, 1103–1123.
(74) Capozzi, B.; Xia, J.; Adak, O.; Dell, E. J.; Liu, Z.-F.; Taylor, J. C.; Neaton, J. B.; Campos, L. M.; Venkataraman, L. Single-Molecule Diodes with High Rectification Ratios through Environmental Control. *Nat. Nanotechnol.* **2015**, *10*, 522–527.
(75) Gutzler, R. Band-Structure Engineering in Conjugated 2D Polymers. *Phys. Chem. Chem. Phys.* **2016**, *18*, 29029–29100.
(76) Dewar, M. J. S.; Kubba, V. P.; Pettit, R. New Heteroaromatic Compounds. Part II. Boron Compounds Isconjugate with Indole, 2 : 3-Benzofuran, and Thionaphthen. *J. Chem. Soc.* **1958**, 3076–3079.
(77) Xu, B.; Tao, N. J. Measurement of Single-Molecule Resistance by Repeated Formation of Molecular Junctions. *Science* **2003**, *301*, 1221–1223.
(78) Venkataraman, L.; Klare, J. E.; Nuckolls, C.; Hybertsen, M. S.; Steigerwald, M. L. Dependence of Single-Molecule Junction Conductance on Molecular Conformation. *Nature* **2006**, *442*, 904–907.
(79) Liu, Z.-F.; Wei, S.; Yoon, H.; Adak, O.; Ponce, I.; Jiang, Y.; Jang, W.-D.; Campos, L. M.; Venkataraman, L.; Neaton, J. B. Control of Single-Molecule Junction Conductance of Porphyrins via a Transition-Metal Center. *Nano Lett.* **2014**, *14*, 5365–5370.
(80) Inkpen, M. S.; Liu, Z.-F.; Li, H.; Campos, L. M.; Neaton, J. B.; Venkataraman, L. Non-Chemisorbed Gold–Sulfur Binding Prevails in Self-Assembled Monolayers. *Nat. Chem.* **2019**, *11*, 351–358.
(81) Soler, J. M.; Artacho, E.; Gale, J. D.; García, A.; Junquera, J.; Ordejón, P.; Sánchez-

Portal, D. The SIESTA Method for Ab Initio Order-N Materials Simulation. *J. Phys. Condens. Matter* **2002**, *14*, 2745–2779.
(82) Perdew, J. P.; Burke, K.; Ernzerhof, M. Generalized Gradient Approximation Made Simple. *Phys. Rev. Lett.* **1996**, *77*, 3865–3868.
(83) Papior, N.; Lorente, N.; Frederiksen, T.; García, A.; Brandbyge, M. Improvements on Non-Equilibrium and Transport Green Function Techniques: The Next-Generation TRANSIESTA. *Comput. Phys. Commun.* **2017**, *212*, 8–24.

For Table of Contents Only